Funneling dynamics in a phenylacetylene trimer: Coherent excitation of donor excitonic states and their superposition

Gabriel Breuil, Etienne Mangaud, Benjamin Lasorne, Osman Atabek, Michèle Desouter-Lecomte

author to whom correspondence should be addressed:michele.desouter-lecomte@universite-paris-saclay.fr

Funneling dynamics in a Phenylacetylene trimer : coherent excitation of donor excitonic states and their superposition

Gabriel Breuil,[1] Etienne Mangaud,[2] Benjamin Lasorne,[1] Osman Atabek,[3] and Michèle Desouter-Lecomte[4]

[1] *ICGM, Univ Montpellier, CNRS, ENSCM, Montpellier, France*
[2] *MSME, Université Gustave Eiffel, UPEC, CNRS, F-77454 Marne-La-Vallée, France*
[3] *Institut des Sciences Moléculaires, Université Paris-Saclay-CNRS, UMR8214, F-91400 Orsay, France*
[4] *Institut de Chimie Physique, Université Paris-Saclay-CNRS, UMR8000, F-91400 Orsay, France*

Funneling dynamics in conjugated dendrimers has raised great interest in the context of artificial light-harvesting processes. Photoinduced relaxation has been explored by time-resolved spectroscopy and simulations, mainly by semiclassical approaches or referring to open quantum systems methods, within the Redfield approximation. Here, we take benefit of an *ab initio* investigation of a Phenylacetylene trimer and in the spirit of a divide-and-conquer approach, we focus on the early dynamics of the hierarchy of interactions. We build a simplified but realistic model by retaining only bright electronic states and selecting the vibrational domain expected to play the dominant role for timescales shorter than 500fs. We specifically analyze the role of the in-plane high-frequency skeletal vibrational modes involving the triple bonds. Open quantum systems non-adiabatic dynamics involving conical intersections is conducted by separating the electronic subsystem from the high-frequency tuning and coupling vibrational baths. This partition is implemented within a robust non-perturbative and non-Markovian method, here the hierarchical equations of motion. We will more precisely analyze the coherent preparation of donor states or of their superposition by short laser pulses with different polarizations. In particular, we extend the π-pulse strategy for the creation of a superposition to a V-type system. We study the relaxation induced by the high-frequency vibrational collective modes and the transitory dissymetry, which results from the creation of a superposition of electronic donor states.

I. INTRODUCTION

The challenge of converting photoexcitation into work has attracted great interest in the context of biological antennae[1–5] or organic photovoltaic devices[6–9]. A crucial debate concerns the role of quantum coherence to explain the performance of the process observed in photosynthetic complexes. The principal questions address different points, namely: the effective role of a coherent transfer versus an incoherent state hopping[10], the nature, purely electronic or vibronic of the coherence[11–14], the influence of the initial preparation to modulate the decoherence. This has given rise to a multitude of experimental works mainly based on two-dimensional spectroscopy[15] and to a lot of theoretical investigations[16–20] in the framework of quantum open systems[21–23]. Indeed, decoherence is a concept that implies separation of a reduced active subspace from residual modes, built in an environment causing dephasing and relaxation. Transfer from an initial donor to a target acceptor involves an excited state gradient leading to the final spatial localization from which the photonic energy may be captured. In a complex molecular system, this corresponds to nonadiabatic transitions among potential energy surfaces possibly through conical intersections[24–30]. A key factor is also the absorption process driving the system from the ground state. Incoherent excitation with sunlight has been examined in many recent works[31–36]. On the other hand, investigation of coherent preparation and control with ultrashort laser pulses remain major issues for modifying the energy transport mechanism[37–39].

Different initializations of the electronic subsystem have been recently compared for a model trimer presenting the so-called Λ scheme between a donor and an acceptor via a bridge[40]. This Λ arrangement should allow a transfer by an adiabatic passage inspired by the STIRAP strategy[41]. In this work, we rather address a V-type system formed by the ground electronic state radiatively coupled to two donor eigenstates, which further decay towards an acceptor state via the bath of vibrational modes. We investigate the particular situation where the transition dipole moments towards the delocalized donor eigenstates are orthogonal such that the states are addressable by laser pulses with different polarizations. This situation differs from dipole alignment, which is a condition for long-lived quasi stationary coherence in a V-type system driven by incoherent light[32]. As recently suggested[39], the relative phase of an initial electronic superposition could then be controlled. In a symmetrical case, choosing the sign of the superposition initializes the system in the left or right zero-order donor sites inducing a transient dissymmetry of the electronic distribution. We compare the efficiency of three strategies for creating this electronic coherence referring either to two linearly polarized pulses or a circularly polarized one, without and with the coupling to vibrational baths.

The selected system presenting this remarkable property with orthogonal transition dipoles is presented in

Fig.1. It consists of a symmetrical trimer of phenylene ethynylene, which is a brick of nanostar dendrimers. Poly(phenylene ethynylene) (PPE) dendrimers are well known as potentially efficient artificial light-harvesting antennae. Such hyper-branched macromolecules are able to collect photons from several peripheral sites. Excitation energy is then funneled towards a focal point or sink from which it is released as useful work, for instance enhanced fluorescence or chemical activation. This unidirectional downhill mechanism has given rise to a large amount of experimental and theoretical investigations[42–50]. In the present example (see Fig.1), the smallest building unit contains two phenylene rings linked by a triple CC bond. The left and right donor chromophores share a common phenylene ring. The acceptor fragment also shares this central part. The trimer architecture (DDA Donor-Donor-Acceptor) may be seen here as the interaction of a symmetrical dimer DD involving two left and right donor sites with a third long acceptor site A. A Frenkel-exciton model is calibrated on such a system by an *ab initio* TD-DFT computation at the CAM-B3LYP/6-31+G* level of theory. A similar *ab initio* investigation of the dimer has been published recently[51].

In open quantum systems, the full electro-nuclear Hamiltonian can be partitioned adequately in several ways, among which two have been abundantly discussed with their *pros* and *cons*[52–60], and in particular in the context of conical intersections[25,30]. The so-called reaction coordinate mapping incorporates some relevant vibrational modes and their couplings through an effective Hamiltonian in the central system. The latter then interacts only with a residual bath usually described by an Ohmic spectral density[52]. The second approach separates the electronic system from all the nuclear motions. The vibrational degrees of freedom are generally assumed to be harmonic and linearly coupled to the electronic degrees of freedom. This is the partition we address here.

We derive a realistic model Hamiltonian for the DDA trimer system by calibrating energies and normal modes from *ab initio* simulations. However, the large coupling of some vibrational modes of this system imposes to work with non-perturbative, non-Markovian dynamical methods. Several methods are available to tackle such dynamics: discretization of the vibrational bath and ML-MCTDH (Multi Layer Multi Configuration Time Dependent Hartree)[61,62], tensor network states[63], the Davydov ansatz[64], or the statistical Schrödinger equation[65,66]. Our choice for this work is the use of HEOM (Hierarchical Equations Of Motion)[67–72]. Four selected electronic states are used to describe the electronic system by a reduced density matrix while the numerous vibrational degrees of freedom (namely, 174) are dealt as several baths at thermal equilibrium. The latter are taken into account with a large set of coupled auxiliary matrices.

The high complexity of dendrimer systems requires multi-scale and multi-method strategies. Here, we take benefit of an *ab initio* investigation of the DDA trimer and in the spirit of a divide-and-conquer approach, we focus on the early dynamics of the hierarchy of interactions. We build a simplified but realistic model by selecting bright electronic states together with the vibrational domain expected to play the leading role for timescales shorter than 500fs. We specifically analyze the role of the in-plane high-frequency skeletal vibrational modes involving the triple bonds. We will more precisely analyze the coherent preparation of donor states or of their superposition by short laser pulses with different polarizations and study the relaxation induced by the high-frequency vibrational collective motions.

This article is organized as follows. In Sec.II, we present the main points of the *ab initio* investigation and we describe the realistic system-bath model calibrated by these data. Sec.III summarizes the HEOM dynamical method. The relaxation mediated by the baths of the system assumed to be prepared in excited donor eigenstates and their superposition is presented in Sec.IV, while Sec.V is devoted to the analysis of the coherent preparation of these states by different laser pulses. Finally, Sec.VI concludes and gives some outlooks.

II. MODEL

A. *Ab initio* computation

All quantum-chemistry calculations were performed with the Gaussian16 package (revision A03)[73] using DFT (ground states) and TD-DFT (excited states) at the CAM-B3LYP/6-31+G* level of theory, the validity of which having been already assessed for the smallest chromophore (tolane) in Ref.[74]. Such calculations were extended to other members of the series: *para*-conjugated PPE oligomers with two, three, and four rings, and we showed in Ref.[75] that the 0–0 band origins and the dominant vibrational progressions were in very good agreement with experimental data. This was further applied to the first *meta*-substituted species in Ref.[51] showing a consistent dimer-like behavior with respect to a pseudo-fragmentation scheme.

Minima and transitions structures were optimised in ground and excited electronic states and characterised with frequency calculations for the system of the present work. Derivative couplings were obtained numerically from the procedure exposed in Ref.[76], based on a harmonic analysis of the Hessian of the squared energy difference.

The ground state geometry is given in the Supplemental Material and a schematic representation of the excited bright states in terms of their dominant excitonic pairs (hole-electron) of natural transition orbitals (NTOs)[77] and their respective weights is provided in Fig.2.

The conical intersection between the two upper excited donor states has been characterized and is schematized in figure 3. The crossing occurs between two states

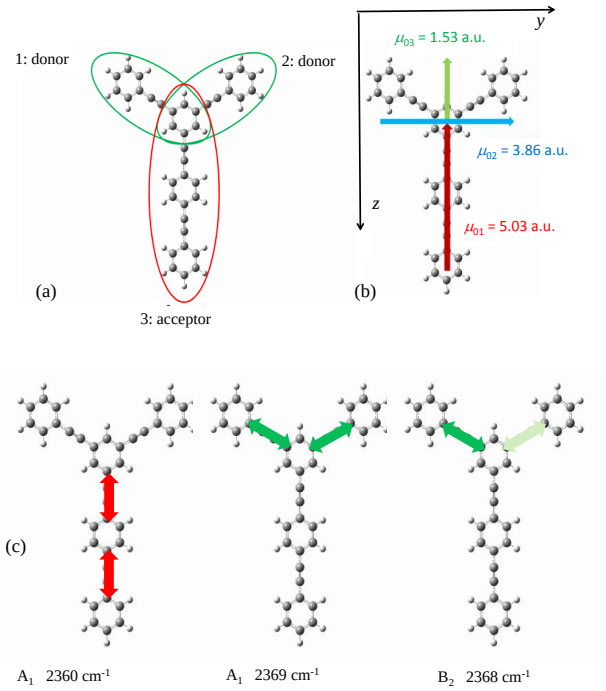

Figure 1. Panel (a): DDA trimer of phenylene ethynylene with a symmetric DD dimer of donor sites 1 and 2 (green circles), and an acceptor A site 3 (red circle). These three sites share a common central ring. The eigenstates mainly localized on the donor sites are denoted E_2 and E_3 in the text. The eigenstate with the main component on the acceptor site is denoted E_1 in the text. Panel (b): The transition dipoles $\mu_{0,k}; k = 1, 2, 3$ from the ground state E_0 are indicated by their corresponding vectors ($k = 1$ in red, $k = 2$ in blue and $k = 3$ in green). The (y, z)-axes are drawn in Mulliken's convention. Panel (c) : Schematic representation of the main in plane skeletal vibrations responsible for the fluctuation of the energy gaps and of the interstate coupling.

Eigenstate	Hole orbital	Electron orbital	Weight
E_1—$^1A_1$	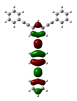	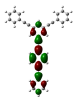	89%
E_2—$^1B_2$	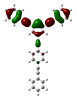	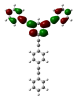	54%
	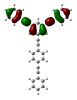	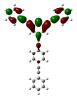	43%
E_3—$^1A_1$	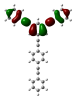	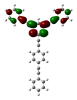	71%
	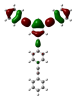	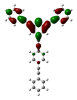	22%

Figure 2. Schematic representation of the three locally excited bright states (acceptor, symmetric donnor, and antisymmetric donnor) in terms of their dominant excitonic pairs (hole-electron) of natural transition orbitals (NTOs)[77] and their respective weights. NTOs are left and right singular vectors of the one-electron reduced transition density; weights are the corresponding singular values.

of different C_{2v} symmetries (namely, A_1 and B_2) and this is the lowest-energy point within the seam due to the positive curvatures of the potential energy surfaces there (except for the coupling mode, of course). Our previous and simpler prototype (two donors connected via meta-substitution) was characterized in the work of Ho *et al.*[75] as a slightly peaked conical intersection with two Transition States (TSs) on both sides along the C_{2v}-preserving coordinate (and two equivalent broken-symmetry, C_s, minima on both sides). Both TSs were very close to the crossing point. Going to the trimer investigated in the present work, we observed a slight shift of the local paraboloids, making the conical intersection now slopped with both apparent minima in C_{2v} on the same side (yet, still close to the crossing) and turning the upper apparent minimum as a true minimum (the lower one still being a TS, unstable with respect to $C_{2v} \rightarrow C_S$, as expected). In both cases, the tilt is not major and the tuning effect is moderate, such that the most important effect is the strong coupling that induces again a symmetric double well, with a pair of C_S mirror-image minima on both sides.

B. Parametrization of the Frenkel Hamiltonian

A minimal model is built by selecting the electronic states and the main vibrational motions expected to play the major role in the early dynamics after preparing donor eigenstates or their superposition. The equilibrium geometry is planar with C_{2v} symmetry. The primary vibrational modes involved in the fluctuation of the energy gaps or of the interstate couplings are the in-plane collective vibrations of the CC triple bonds with A_1 or B_2 symmetry around 2360 cm^{-1}. The electronic subspace is limited to the ground electronic state and the first three bright states. We neglect the presence of dark states, which nevertheless could participate to a more sophisticated relaxation mechanism, left for further work. The ground adiabatic state E_0 is cou-

pled to the excited bright states only through transition dipole moments. In other words, in the absence of non-radiative transitions, E_0 could be qualified both as adiabatic and diabatic. The first excited state E_1 (A_1) is the acceptor. The higher excited states E_2 (B_2) and E_3 (A_1) are the donors, which may be seen in first approximation as the in- and out of-phase combinations of the localized electronic states of the two left and right donor sites. According to the usual model of displaced harmonic oscillators in open quantum systems, we work with a linear vibronic Hamiltonian expressed in a diabatic representation. The equilibrium geometry of the ground electronic state (*i.e.,* the Franck-Condon geometry) fixes the spatial origin of the normal modes. They are assumed to be the same in each excited diabatic state by neglecting the Duschinsky rotation. A generic field-free Frenkel Hamiltonian then reads:

$$H = \sum_k |k\rangle H_{kk} \langle k| + \sum_{j\neq k} |j\rangle H_{jk} \langle k| \tag{1}$$

which, in mass weighted coordinates, leads to:

$$H_{kk} = \varepsilon_k + 1/2 \sum_\alpha \left(p_\alpha^2 + \omega_\alpha^2 (q_\alpha - d_\alpha(k))^2 \right) \tag{2}$$

and

$$H_{jk} = h_{jk} + \sum_\alpha \kappa_a(jk) q_\alpha \tag{3}$$

where ϵ_k is the electronic energy at the equilibrium geometry of the ground state and h_{jk} is the electronic coupling between states j and k. The minimum energy of state k is displaced by $d_\alpha(k)$ with respect to the equilibrium position of mode q_α in the ground state. In the harmonic model, $c_\alpha(k) = -\omega_\alpha^2 d_\alpha(k)$ is the gradient at the reference point $q_\alpha = 0$ and $\kappa_\alpha(jk)$ is the gradient of the interstate coupling. The sum $\varepsilon_k + 1/2 \sum_\alpha \omega_\alpha^2 d_\alpha^2(k)$ gives the energy at the reference Franck-Condon geometry and $\lambda_k = 1/2 \sum_\alpha \omega_\alpha^2 d_\alpha^2(k)$ is the reorganization (renormalization) energy.

The system-bath-type Hamiltonian is recast as:

$$H = H_S + H_{SB} + H_B \tag{4}$$

where H_S is the quantum subsystem explicitly treated. Here, we address the specific partition where H_S is the electronic Hamiltonian at the minimum of the ground electronic state. The diabatic electronic representation is not unique since it is defined, formally, at least up to an arbitrary unitary transformation that does not depend on the nuclear coordinates (and depends, in practice, also on the specific choice of some diabatic criterion among various and equally valid possibilities)[78–80]. Some diabatic basis sets may be more suitable for discussing the vibronic couplings, in particular in the context of conical intersections. Two particular diabatic representations and the adiabatic states of the two donor states are represented in Fig. 3. We denote H^d the Hamiltonian expressed in the basis set formed by the delocalized states adapted to C_{2v} symmetry (Fig. 2, left panel). These states denoted D_2 and D_3 have the same symmetry as the adiabatic states E_2 (B_2) and E_3 (A_1), respectively. Their coupling vanishes in A_1 geometry but their energy gap is varying, so that an A_1 displacement is a tuning mode. However, they exhibit a linear coupling along B_2 displacements leading after diagonalization to a double well profile for the lower E_2 adiabatic state. At the Franck-Condon geometry, the electronic matrix H_S^d is:

$$H_S^d = \begin{pmatrix} E_0 & 0 & 0 & 0 \\ 0 & \varepsilon_A & 0 & h^d_{AD_3} \\ 0 & 0 & \varepsilon_{D_2} & 0 \\ 0 & h^d_{D_3 A} & 0 & \varepsilon_{D_3} \end{pmatrix}. \tag{5}$$

Transforming through a $\pi/4$ rotation matrix $R(\pi/4)$, mixes D_2 and D_3 while leaving E_0 and A unchanged. One gets the Hamiltonian $H_S^l = R^t(\pi/4) H_S^d R(\pi/4)$ in a basis set localized on the left or right donor sites:

$$H_S^l = \begin{pmatrix} E_0 & 0 & 0 & 0 \\ 0 & \varepsilon_A & h^l_{AD_L} & h^l_{AD_R} \\ 0 & h^l_{AD_L} & \varepsilon_D & h^l_{D_l D_R} \\ 0 & h^l_{AD_R} & h^l_{D_l D_R} & \varepsilon_D \end{pmatrix}. \tag{6}$$

In the DD dimer case, without interaction with the third site, the minima of the diabatic states D_L and D_R should coincide with those of the double well adiabatic state along a B_2 displacement. Their energy gap is varying along the B_2 motion while they are degenerate along A_1. $\varepsilon_{D_L} = \varepsilon_{D_D} = \varepsilon_D$ and $h^d_{AD_3} = \sqrt{2} h^l_{AD_L} = \sqrt{2} h^l_{AD_R}$. The role of tuning and coupling modes are exchanged due to the rotation $R(\pi/4)$ of the electronic reduced basis set. The operators H_{SB} and H_B must be adapted to the chosen basis set. Computations are performed in the delocalized basis set which is transformed to the localized one for some analysis. Energies and couplings in Eqs.(5, 6) are ideally obtained from *ab initio* adiabatic calculations. However, realistic assumptions are made when we are missing some of them. More precisely, without coupling between the DD dimer and the third A site, the diabatic energies of the delocalized basis set should be the adiabatic ones in C_{2v} symmetry. One may expect that the coupling $h^l_{AD_{D/R}}$ has a value in the range $\left[0, h^l_{D_L D_R}\right]$. By a best fit procedure, we determined reasonable diabatic values $\varepsilon_0 = 0$, $\varepsilon_A = 3.8613$ eV, $\varepsilon_{D_2} = 4.3897$ eV, $\varepsilon_{D_3} = 4.4678$ eV and $h^d_{AD_3} = 0.03025$ eV that provide the following adiabatic energies at the Franck-Condon geometry: $E_0 = 0$, $E_1 = 3.8589$ eV, $E_2 = 4.3895$ eV, $E_3 = 4.4698$ eV (These values are to be compared with the *ab initio* calculated ones: $E_1 = 3.8598$ eV, $E_2 = 4.3897$ eV, $E_3 = 4.4692$ eV respectively).

The bath is a collection of harmonic oscillators representing the discrete intramolecular vibrational modes as well as the effect of an environment. In the framework of conical intersections with symmetry properties,

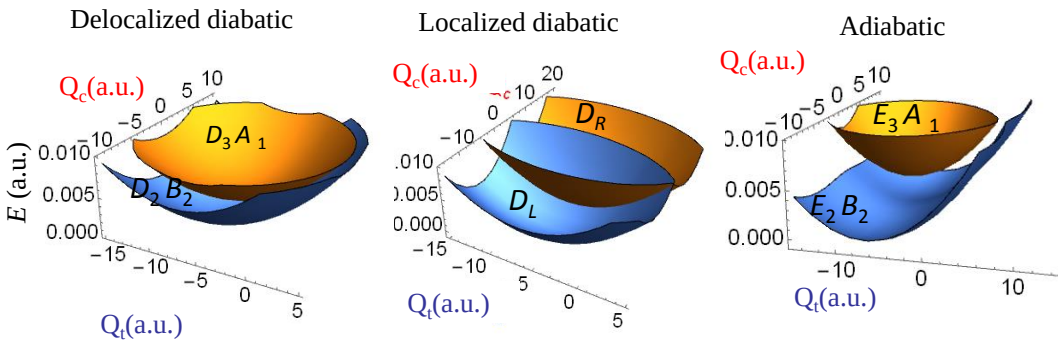

Figure 3. 3D-schematic view of the potential energy surfaces of the diabatic harmonic model. Delocalized diabatic donor states D_2 and D_3 (left panel), localized diabatic states D_L and D_R (middle panel) and adiabatic states (right panel). The tuning mode (coordinate Q_t) is the vibrational mode of A_1 symmetry at 2369 cm^{-1} and the coupling mode (coordinate Q_c) is the vibrational mode of B_2 symmetry at 2368 cm^{-1}. Energy minima were obtained from *ab initio* data.

the modes are usually separated into tuning type modes coupled to the diagonal elements of H_S, and coupling type modes which are off-diagonally coupled[25,30,81–84]. The system-bath coupling is $H_{SB} = \sum_n S_n \otimes B_n$ where S_n and B_n are operators acting in the space of the electronic system or in the complementary vibrational space, respectively. The B_n operator corresponds to a collective mode having the dimension of an energy. n is a generic index equal to k for the tuning baths affecting the diagonal elements and jk for the coupling baths linked to the off-diagonal elements. For the tuning mode,

$$B_k^{diag} = \sum\nolimits_\alpha c_\alpha(k) q_\alpha = -\sum\nolimits_k \omega_\alpha^2 d_\alpha(k) q_\alpha \qquad (7)$$

where the vibronic couplings $c_\alpha(k)$ are the gradients at the reference point (see Eq.(2)). For the coupling modes (off-diagonal part),

$$B_{jk}^{off} = \sum\nolimits_\alpha \kappa_\alpha(jk) q_\alpha \qquad (8)$$

where $\kappa_\alpha(jk)$ are the linear interstate couplings (Eq.(3)). In this application, the tuning-type (Eq.(7)) and coupling-type (Eq.(8)) collective modes are orthogonal since they involve subsets of modes belonging to different symmetries. If this were not the case an orthogonalisation procedure has to be used as referred to in references[82,83]. Finally, figure 4 summarizes the parameters of the system-bath model.

C. Parametrization of the baths

The tuning baths make the energies fluctuate and are linked to the diagonal elements of H_S^d. They are denoted by a single index $k = A, D_2, D_3$. On the contrary, the coupling baths connect two states and are denoted by the corresponding pair of indices,

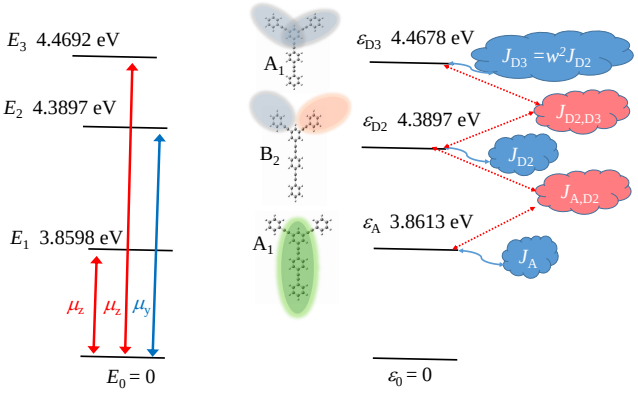

Figure 4. Schematic representation of the system-bath model providing the adiabatic energies E_j, the energies of the delocalized diabatic representation ϵ_j, and the allowed dipolar transitions (red, along z-axis; blue, along y-axis). Are also indicated on the right panel: (in blue) the couplings to the tuning baths J_k for $k = A$, D_2 and D_3, (the parameter w is discussed in the text, here $w = = 0.77$), and (in red) those to the coupling baths $J_{D_2D_3}$ and J_{AD_2}.

namely: $jk = AD_2, D_2D_3$. The corresponding collective bath modes are defined in Eqs.(7) and (8). The fluctuation-dissipation induced by the baths is described by two-point correlation functions of the collective modes $C_{nm}(t) = \langle B_n(t) B_m(0) \rangle_{eq}$ (n and m being collective indexes equal to k for the tuning modes or kk' for the coupling modes) where $B_n(t)$ is the Heisenberg representation of the operator and $\langle \bullet \rangle_{eq} = Tr_B[\bullet \rho_B^{eq}]$ denotes the average over a Boltzmann thermal ensemble of harmonic oscillators at temperature T. These correlation functions of collective modes are a basic tool in open quantum systems[85] and in particular, they have been used in the context of the hierarchical representation of the sepctral density in master equations[86,87]. They are related to the spectral densities through a temperature-

dependent modified Fourier transform:

$$C_{nm}(t) = 1/\pi \int_{-\infty}^{\infty} d\omega J_{nm}(\omega)\,[f(\omega)+1]e^{-i\omega t} \qquad (9)$$

where $f(\omega) = \left(e^{\beta\omega}-1\right)^{-1}$ is the Bose function, $\beta = 1/k_BT$ and $J_{nm}(-\omega) = -J_{nm}(\omega)$. In a discrete representation the spectral density may be expressed from the system-bath coupling coefficients $c_\alpha(k)$ or $\kappa_\alpha(jk)$. For the tuning baths, one has:

$$J_{k,k'}(\omega) = \frac{\pi}{2}\sum\nolimits_\alpha \frac{c_\alpha(k)c_\alpha(k')}{\omega_\alpha}\delta(\omega-\omega_\alpha). \qquad (10)$$

and accordingly, for the coupling modes:

$$J_{jk,j'k'}(\omega) = \frac{\pi}{2}\sum\nolimits_\alpha \frac{\kappa_\alpha(jk)\kappa_\alpha(j'k')}{\omega_\alpha}\delta(\omega-\omega_\alpha). \qquad (11)$$

We recall that the diagonal terms are denoted with a single index when $k' = k$ in Eq.(10) or $j'k' = jk$ in Eq.(11).

1. *Tuning baths*

For independent baths, the operators corresponding to tuning ones are merely $S_k = |k\rangle\langle k|$, whereas they are written $S_{kj} = |k\rangle\langle j|$ for coupling baths. In cases where off diagonal terms $C_{kk'}(t)$ (or $J_{kk'}(\omega)$) with $k' \neq k$ cannot be discarded, baths are correlated. Some recent works have addressed such situations leading to more complicated dynamical treatments[88–90]. There are however some circumstances under which the correlation of two baths 1 and 2 could be implicitly taken into account by referring to a single bath, but a different S operator[88]. Two baths should be perfectly correlated or anti-correlated if the variation of a given important mode affects the system-bath coupling in a similar way, *i.e.,* $c_\alpha(k') = c_\alpha(k)$, or in an opposite way, *i.e,* $c_\alpha(k') = -c_\alpha(k)$, respectively. In other words, the gradients are then the same or have opposite directions in the two electronic states. The operator linked to the single bath then reads $|1\rangle\langle 1| + |2\rangle\langle 2|$ or $|1\rangle\langle 1| - |2\rangle\langle 2|$ respectively. Upon assuming the relation $c_\alpha(k') = wc_\alpha(k)$, it is possible to work with a single bath described by the spectral density J_{kk} and a composite operator $S = |k\rangle\langle k| + w\,|k'\rangle\langle k'|$. This may be verified for instance by considering the HEOM equations at the first level, which correspond to the generalized Bloch-Redfield equations at the second order of perturbation[57].

We estimate the coefficients $c_\alpha(k) = -\omega_\alpha^2 d_\alpha(k)$ in the delocalized basis set (Eq.(5)). This is done by assuming that the DD donor dimer is weakly coupled to the A acceptor site. The gradient of each potential electronic surface at the Franck-Condon geometry and minima displacements from that geometry are extracted from *ab initio* computations. Vibronic couplings can be obtained from both quantities and the agreement between both approaches is a test of the harmonic and linear coupling approximations. For the D_2 and D_3 states, the displacements are from the Franck-Condon geometry to the minimum in the A_1 geometry. For D_3, this minimum corresponds to the Transition State with respect to the B_2 modes.

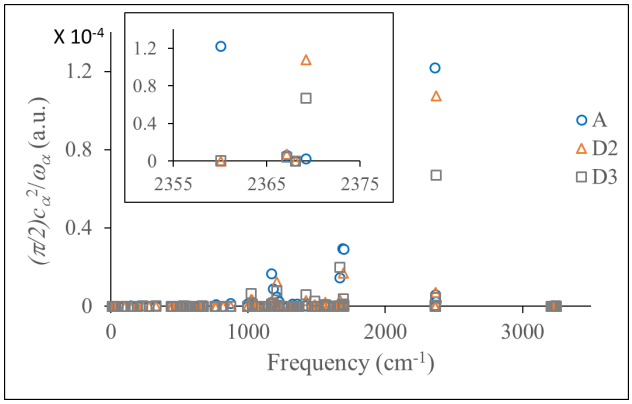

Figure 5. Contribution of the intramolecular modes to the discrete spectral densities J_k (Eq.10) for $k = A$ (blue circle), D_2 (red triangle) and D_3 (black rectangle). The inset is an enlargement on the frequency domain corresponding to the vibration of the CC triple bonds.

The discrete contributions $c_\alpha^2(k)/\omega_\alpha$ to the spectral densities of the three tuning baths A, D_2 and D_3 are given in Fig. 5. The dominant intramolecular motions leading to the highest couplings are the vibration of the CC triple bonds around 2360 cm^{-1}. The strength of the vibronic coupling could also be estimated by the dimensionless Huang-Rhys factor $s_\alpha(k) = \omega_\alpha d_\alpha^2(k)/2\hbar$. The weighting by the frequencies is then different but the selected high-frequency range remains the most coupled to the system. The zoom in the inset of figure 5 shows that the mode at 2369 cm^{-1} induces large coefficients for both D_2 and D_3 states. This is an example of the relation $c_\alpha(D_3) = wc_\alpha(D_2)$ discussed above. On the contrary, the tuning bath of state A is dominated by the vibration at 2360 cm^{-1} where the contribution of other two states are negligible. As we focus on this high-frequency domain, the tuning bath A is therefore considered as independent ($S_A = |A\rangle\langle A|$ while the tuning baths D_2 and D_3 are treated as correlated with a single operator $S = |D_2\rangle\langle D_2| + w\,|D_3\rangle\langle D_3|$ with $w = 0.77$.

The discrete spectral density and undamped oscillators could be directly used as it has been done in simulations with ML-MCTDH[61,62], Thermo Field Dynamics[91] and HEOM[71,92,93]. However, the benchmark examples mainly concern dynamics in the Fenna-Matthews-Olson (FMO) complex where the system-bath coupling remains weak and does not involve high levels of hierarchy. The system-bath partition adopted here leads to very strong coupling in the context of conical intersection and high hierarchy level. We prefer to take benefit of a simple model based on a continuous representa-

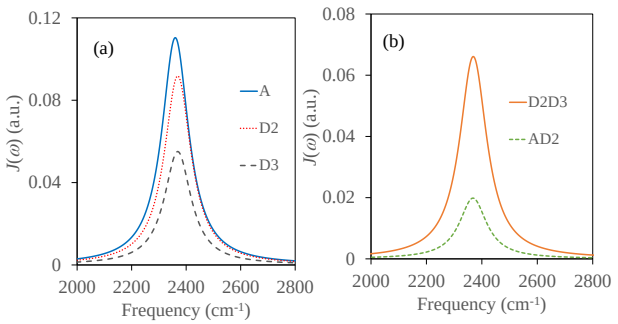

Figure 6. Spectral densities in the high-frequency range of the skeletal CC triple bonds smoothed by Tannor-Meier Lorentzians (Eq.(12)). Panel (a): spectral densities J_k for the tuning baths $k = A$, D_2 and D_3; panel (b) : spectral densities J_{jk} of the coupling baths $jk = D_2D_3$ and AD_2 .

tion of the spectral density (Eq. 10) already used in a previous work[30]. The delta distribution in the spectral density is broadened by a Lorentzian smoothing function $\delta(\omega-\omega_k) \to \frac{1}{\pi}\frac{\Gamma}{(\omega-\omega_k)^2+\Gamma^2}$[90,94,95]. In this work, we used $\Gamma = 160$ cm^{-1}. Truncating to the high-frequency domain, the sharp peaks are fitted by two-pole Tannor-Meier Lorentzians[96] represented in Fig. 6(a).

$$J_{nm}(\omega) = \sum\nolimits_j \frac{p_j\omega}{\left[(\omega+\Omega_j)^2+\Gamma_j^2\right]\left[(\omega-\Omega_j)^2+\Gamma_j^2\right]}. \tag{12}$$

The parameters are given in Appendix A.

2. *Coupling baths*

The linear coupling coefficients $\kappa_\alpha(D_2D_3)$ (Eq.(8)) of the delocalized donor states D_2 and D_3 may be estimated from some adiabatic data in the harmonic model. As schematized in Fig.3, the energy gap between the delocalized diabatic states is varying along a tuning mode but is constant along any coupling mode, which breaks the symmetry. The linear coupling leads to a lower adiabatic state that may present a double-well shape when the coupling is strong. The *ab initio* data provide the geometry of these minima in the restricted planar geometry we consider here. For each vibrational mode, the linear coupling gradient may be estimated from the analytic expression of the lower adiabatic state, by imposing that the first derivative of this adiabatic energy vanishes at the local minimum. It is this approximate procedure that we have adopted. For the largest off-diagonal linear coupling terms aimed at inducing both equivalent minima in E_2, we have compared their agreement to a direct evaluation according to the numerical procedure described in Ref.[76]. The agreement justifies the harmonic and linear approximation. The spectral density is then obtained by a Lorentzian smoothing function, in the same way as for the tuning baths. It presents a sharp peak centered at the B_2 vibrational mode at 2368 cm^{-1}, which is the antisymmetric vibration of the triple bonds in the two right and left sites. The parameters of the Tannor-Meier Lorentzian are given in Appendix A.

The coupling between the A and D_2 states vanishes in C_{2v} symmetry (see Eq.(5)). However, it does not cancel when B_2 vibrations are activated. At this stage, our use of local *ab initio* energies and derivatives is not global enough to precisely fix the linear coefficients $\kappa_\alpha(AD_2)$. One may reasonably assume that they are smaller than the corresponding $\kappa_\alpha(D_2D_3)$. We consider that the coupling baths are uncorrelated and that the spectral densities are related by $J_{AD_2} = w' J_{D_2D_3}$ with a factor $w' = 0.3$. We give in the supplemental material a comparison of dynamics carried out with $w' = 0.1$ and $w' = 0.5$ to illustrate the qualitative stability of the results. Finally, the weak interaction between the A and D_3 states, which does not vanish in C_{2v} symmetry, is taken as a small constant.

III. DYNAMICAL METHODS

We summarize hereafter the main equations of the HEOM formalism,which is currently well documented[67–72]. In the case of independent baths or when the correlation may be treated by a composite operator as discussed in section II C, only the diagonal correlation functions of the baths are required. As in Sec.II, the diagonal elements will be denoted by a single bath index $C_j(t) = C_{jj'}(t)\delta_{jj'}$ where $j = A, D2, D3$ for the tuning baths and $j = D_2D_3, AD_2$ for the coupling baths. The efficiency of the algorithm relies on the expansion of the correlation functions $C_j(t)$ as a sum of $n_{ncor,j}$ complex exponential functions associated to pseudo decay modes. Different expansions have been proposed[71] among which the Tannor-Meier scheme[96,97], the Padé approximation[98], the Fano spectrum decomposition[99] and an expansion on Chebyshev polynomials and Bessel functions[100]. According to the Tannor-Meier method, the correlation function is written as :

$$C_j(t) = \sum_{l_j=1}^{n_{cor,j}} \alpha_{j,l_j} e^{i\gamma_{j,l_j}t} \tag{13}$$

Expressions for α and γ as functions of the parameters of the spectral density (12) are given in Refs.[96,97].

The reduced density matrix of the system

$$\rho_S(t) = Tr_B\left[\rho_{tot}(t)\right] \tag{14}$$

is the partial trace over the bath of the time evolution of the total density matrix $\rho_{tot}(t)$. The auxiliary operators are matrices of the same dimension as the system density matrix. They are denoted by a collective index $\mathbf{n}$ giving the excitation number in the pseudo modes of each correlation function, $\mathbf{n} =$

$\{n_{1,1},\cdots,n_{n_{cor,1}},\cdots,n_{1,j},\cdots,n_{n_{cor,j}},\cdots\}$. The equations in interaction representation take the form[30]

$$\begin{cases} \dot{\rho}_{S,I}(t) = \sum_{k=1}^{K} \Phi_j(t)\rho^{(1)}_{0_1,\cdots,0_k+1,\cdots,0_K}(t) \\ \dot{\rho}^{(\nu)}_{n_1,\cdots,n_K}(t) = \sum_{k=1}^{K} \Phi_j(t)\rho^{(\nu+1)}_{n_1,\cdots,n_k+1,\cdots,n_K}(t) \\ \qquad + \sum_{k=1}^{K} n_k\Theta_k\left(t\right)\rho^{(\nu-1)}_{n_1,\cdots,n_k-1,\cdots,n_K}(t) \\ \qquad + i\sum_{k=1}^{K} n_k\gamma_k\rho^{(\nu)}_{n_1,\cdots,n_K}(t). \end{cases} \tag{15}$$

where

$$\Phi_j(\tau)\centerdot = -[S_j(\tau),\centerdot] \tag{16}$$

and

$$\Theta_k(t')\centerdot = \alpha_{j,l_j}S_j\left(t'\right)\centerdot - \tilde{\alpha}_{j,l_j}\centerdot S_j\left(t'\right). \tag{17}$$

$\rho_{S,I}(t) = \rho^{(0)}_{0,\cdots,0}(t)$ is the reduced density matrix for the system in interaction representation. Expressions for $\tilde{\alpha}$, which are related to the complex conjugate of the correlation function, are given in Ref.[97]. $k = \{l_j, j\}$ is a global index related to an exponential element l_j of the j's bath correlation function. K is the total number of exponential functions involved in all the correlation functions. (ν) is the hierarchy level of the matrix defined such that $\nu = \sum_{i=1}^{K} \mathbf{n}_i$.

The HEOM formalism provides insight on the correlated system-bath dynamics by probing the different moments $X_j^{(n)}(t) = \mathrm{Tr}_{B_j}\left[B_j^{(n)}\rho_{tot}(t)\right]$ of the collective mode B_j of the tuning (Eq.7) and coupling (Eq.8) baths[30,71,101,102]. The first moment $X_j(t)$ will be denoted without its exponent ($n = 1$). The expectation value of the collective mode B_j in each electronic state m is given by the m^{th} diagonal elements of the matrix $X_j(t)$, which in turn is given by the sum of the first level auxiliary matrices

$$X_j(t) = -\sum\nolimits_{\mathbf{n}'} \rho_{\mathbf{n}'}(t) \tag{18}$$

where the sum runs over all index vectors belonging to level 1 of the hierarchy, i.e. $\sum_{k=1}^{n_{cor,j}} n_{k,j} = 1$ and $\sum_{k=1}^{n_{cor,j'}} n_{k,j'} = 0$ with $j' \neq j$. This first moment already provides a signature of the induced correlated system-bath dynamics, in particular of the damped vibrational motion in the successive electronic states during the relaxation. In order to get the dimension of a coordinate, the moment is divided by the total coupling strength of the corresponding bath $X_j(t)/D_j$ with

$${D_j}^2 = 2/\pi \int_0^\infty J_j(\omega)\omega d\omega. \tag{19}$$

The investigation of the full distribution, which should correspond to the distribution extracted from wave packet dynamics in the alternative partition retaining the collective coordinates into the active system, has been illustrated recently[30,102].

The equations at $T = 298$K are solved by the Cash-Karp Runge Kutta adaptative algorithm[103] with a filter procedure in order to reduce the number of auxiliary matrices. Convergence is reached at level 8 with two Matsubara matrices for each bath. We give the results obtained without Matsubara terms since we have checked on several cases that the error is less than 1%. For computational purposes, we adapt a filtering strategy proposed by Q. Shi[70] to our algorithm in order to reduce the computational cost. Connectivity between auxiliary matrices (up to the 8th level in this case) is determined as a first computational step. At each integration step, an algorithm computes $\zeta_k = \sqrt{\max(|[\rho^{(\nu_t)}_{n_1,\ldots,n_K}]_{ij}|)}$ where $\nu_t(>=0)$ indexes the current upper hierarchical level at time t (at $t = 0$, $\nu_t = 0$), i,j are elements of the auxiliary density matrices and k is an index of density matrix with $\sum n_k = \nu_t$. If $\zeta_k > \epsilon_f = 1.\times 10^{-9}$, all auxiliary matrices' set of equations connected to k are allowed to be solved. This procedure is iterated up to convergence for each integration step. By keeping ϵ_f sufficiently small, one can ensure a numerically exact resolution of HEOM equations while reducing the effective cost of the computation. Indeed, at each step t, only a limited number of auxiliary matrices contribute to the reduced density matrix. This procedure has been checked with several ϵ_f parameters.

IV. FIELD-FREE RELAXATION DYNAMICS

We first examine the relaxation process when the system is assumed to be prepared in the excited donor eigenstates. As the radiative coupling is not introduced in this work, the final state is the acceptor E_1. Fig. 7 gives the adiabatic population evolution, when dynamics are initiated in state E_3 (panel a), E_2 (panel b) or in their superposition with equal weights (panel c). The decay of both donor states is complete in about 250fs and the acceptor yield reaches 90% in about 100fs. The funneling mechanism from E_3 towards E_1 through E_2 is clearly seen in Fig.7(a) since population in E_1 increases when E_2 accumulates population and the relaxation slows down during the transitory return from E_2 to E_3. Fig.7(c) gives the population evolution of the superposition. The population relaxation does not differ from that of a mixture of both states with equal weights. The difference is less than 1%. In the present case, the initial electronic coherence decays in about 25 fs and it does not influence the decay rate towards the acceptor. However, dynamics is not the same with respect to the occupation of the donor left and right sites. An initial superposition $|\pm\rangle = \left(|2\rangle \pm |3\rangle\right)/\sqrt{2}$ corresponds to an initial population in one or the other localized diabatic states $|D_R\rangle$ or $|D_L\rangle$. This leads to an early vibrational displacement towards the right or left minimum followed

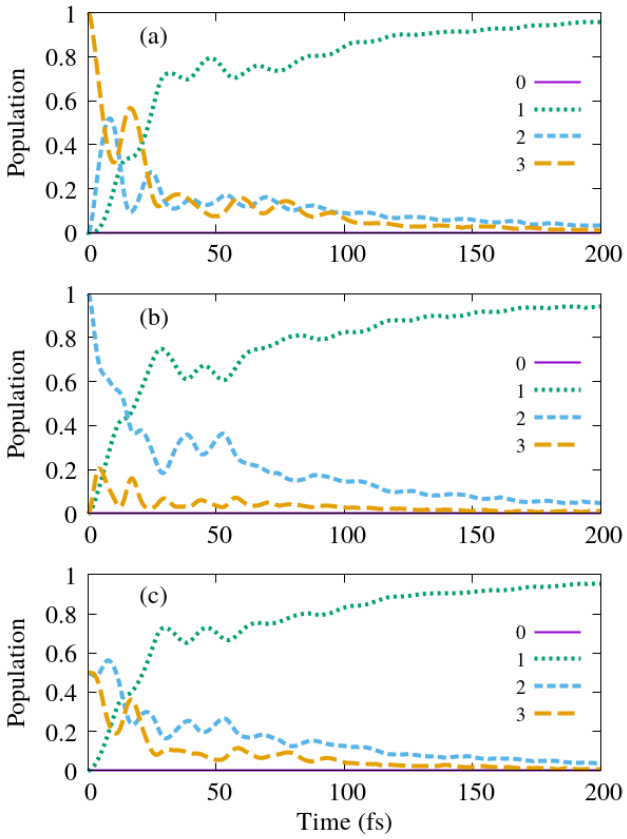

Figure 7. Adiabatic populations as a function of time: Solid line (magenta) for E_0 (zero), dotted line (green) for E_1, dashed line (blue) for E_2 and long-dashed line (orange) for E_3. The system is assumed to be prepared in donor states E_3 (panel a) or E_2 (panel b) or in the superposition $|\pm\rangle = (|2\rangle \pm |3\rangle)/\sqrt{2}$ (panel c).

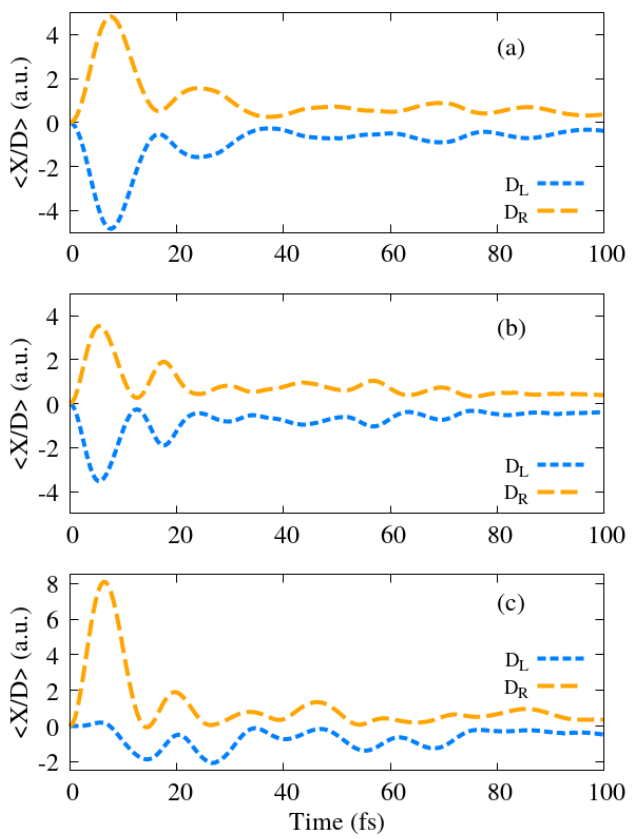

Figure 8. Evolution of the average value of the collective vibrational mode of the coupling bath $J_{D_2D_3}$ (Eqs.(18) and (19)) in the localized diabatic states D_L (dashed line (blue)) or D_R (long-dashed line (orange)) when the system is assumed to be prepared in the different states. Panel (a) : initial state E_3, panel (b) : initial state E_2, panel (c) : initial superposed state $|+\rangle = (|2\rangle + |3\rangle)/\sqrt{2}$. The opposite sign is obtained for $|-\rangle = (|2\rangle - |3\rangle)/\sqrt{2}$

by a damped oscillation between the two wells. This asymmetry is typical of the superposition since preparing an eigenstate or a mixture with equal weights gives an equal population in both localized wells and therefore a simultaneous motion towards both minima.

Insight into the vibrational motion is provided by the average value of the collective bath modes (Eq.18), which may be computed in any adiabatic or diabatic representation. X/D (Eqs.(18,19)) in a given electronic state corresponds to the mean position of the component of a nuclear wave packet evolving on the coupled potential energy surfaces. One may observe the damped oscillatory motion. The average goes to zero when the norm of the component vanishes due to nonadiabatic transitions. We first focus on the coupling mode of states E_2 and E_3 in the delocalized diabatic representation. Fig. 8 displays the average position in states D_L and D_R when the system is prepared either in state E_3 (panel (a)), E_2 (panel (b)), or in their superposition $|+\rangle = (|2\rangle + |3\rangle)/\sqrt{2}$ (panel (c)). In the first two cases (a) and (b), the symmetry leads to a simultaneous occupation of each left or right donor monomer. In the adiabatic representation where the potential energy surfaces are symmetrical, the average position is always zero due to symmetry. The excitation of the superposed state (panel (c)) clearly induces a transitory occupation of a single left or right well. The large initial asymmetry subsists for about 10fs only and it leads to subsequent damped oscillations between the two wells. Obviously, in the present example, a damped oscillatory behavior due to the coherent superposition or a smooth decay of a uniform population of both wells in a mixture induces a similar decay towards the acceptor.

To have a similar analysis on the vibrational motion of the tuning modes, we go back to the adiabatic representation and we illustrate the evolution towards equilibrium when the system is prepared in the upper donor adiabatic state E_3. Fig.9 displays the average position (Eqs.(18,19)) of the collective vibrational mode of different baths during the early dynamics. Panel (a) gives the evolution of the collective tuning mode of the acceptor bath J_A. The mean position slightly oscillates around the Franck-Condon geometry in the donor states and stabilizes at zero when the population vanishes. For

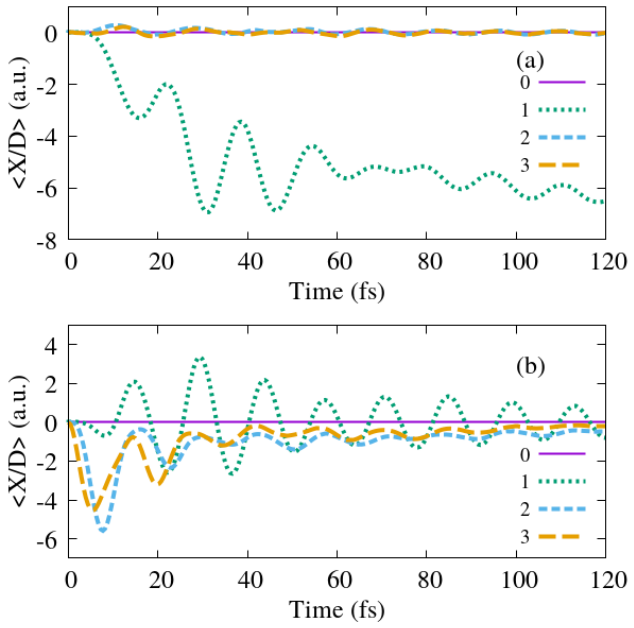

Figure 9. Evolution of the average value of the collective vibrational tuning modes (Eqs.(18) and (19)) in the adiabatic states when the system is assumed to be prepared in the donor state E_3. Panel (a) : tuning mode of bath J_A, panel (b) : tuning mode of bath J_{D_2}. The color code is the same as in Fig.7.

this bath one may see the damped oscillations of the component in E_1, which relaxes towards the new equilibrium position of the acceptor. As illustrated in panel (b), the bath J_{D_2} mainly affects the two donor states, which have the same tuning mode. One observes the first large oscillation towards the equilibrium position of these states before the collapse due to the transition towards E_1. This tuning mode for E_2 and E_3 is not the tuning mode for E_1 and the motion in this state results in a damped oscillation around the Franck-Condon geometry.

The stability of the dynamics with respect to the spectral density range is verified in the Supporting Information where we systematically add one or two regions corresponding to the secondary maxima around 1700 cm^{-1} and 1200 cm^{-1} depicted in Fig. 5 in the acceptor or in the donor baths. This confirms that the early relaxation is mainly driven by the triple bond high frequency stretches, as already observed in semiclassical simulations[104]. Consideration of the low frequencies for the coupling baths is more problematic and will probably require the inclusion of out-of-plane motions.

V. COHERENT EXCITATION OF THE DONOR STATES

We now discuss the effect of some coherent excitations towards the donor states from the ground state with laser pulses to decipher the role of the baths and of the different polarisations. State E_2 is excited through a transition dipole $\mu_{y,02} = 3.86$ a.u. along Oy axis, and state E_3 through $\mu_{z,03} = 1.58$ a.u. along Oz axis (see Figs.1 and 4). Our primary concern is not the population control of the bright acceptor state that could otherwise be excited directly from the ground state through $\mu_{z,03} = 5.47$ a.u. We rather put the emphasis on the general tendencies and the characteristic timescales of such field-driven dynamics, and in particular on a preparation of a superposed state implying the two donors.

The trimer is studied in planar geometry and assumed to be oriented in the plane Oyz orthogonal to the propagation direction Ox of the electromagnetic waves, as indicated in Fig.1. The time-dependent system Hamiltonian becomes $H_S(t) = H_S + V(t)$ where the interaction with the electromagnetic field $\vec{\mathcal{E}}(t)$ is written in length gauge and within the dipole approximation as:

$$V(t) = -\vec{\mu}\vec{\mathcal{E}}(t) = -\mu_y\mathcal{E}_y(t) - \mu_z\mathcal{E}_z(t). \qquad (20)$$

The transition dipole matrices are computed in the adiabatic representation and transformed to the delocalized diabatic basis for the dynamical treatment. They are given in Appendix A. A pulse linearly polarized along Oy or Oz induces the $E_0 \rightarrow E_2$ or $E_0 \rightarrow E_3$ transition respectively. However, for strong fields polarized along Oz one can also expect an interference with the transfer $E_0 \rightarrow E_1$. Spontaneous radiative decay is not included in the simulations. We address the preparation of the donor states E_2 or E_3 or of their superposition $|\pm\rangle = (|2\rangle \pm |3\rangle)/\sqrt{2}$, in other words, in the left or right donor site, D_L or D_R. In the following, we examine different excitation strategies, referring to appropriately shaped pulsed lasers, with different polarizations.

A. Excitation of a single eigenstate

Simple strategies leading to analytical solutions are available for the bath-free electronic system for two- or three-state models. However, these simple schemes are perturbed by possible interference with detuned transitions in the complete basis set or by the baths, *i.e.*, by the vibronic couplings, which make fluctuate the energy gaps. These are precisely the effects we intend to analyze in the following.

A π-pulse is such a possible strategy[105,106]. The pulses polarized along Oy or Oz are assumed to have a sine square envelope and the carrier frequency is in resonance with the transition towards the selected donor state. The electric field amplitude reads:

$$\mathcal{E}_{y/z}(t) = \mathcal{A}_{y/z}(t)\cos\left(\omega_{y/z}t + \phi_{y/z}\right) \qquad (21)$$

with

$$\mathcal{A}_{y/z}(t) = A_{y/z}\sin^2\left(\frac{\pi t}{\tau_{\max}}\right). \qquad (22)$$

In a two-state case, the transfer is complete if the integral of the Rabi frequency $\Omega_{y/z}(t) = \mu_{0,2/3}\mathcal{A}_{y/z}(t)/\hbar$

over the pulse duration τ_{max} is equal to π. With the sine square envelope, the field amplitude is then related to the pulse duration by $A_{y/z} = 2\pi/\mu_{0,2/3}\tau_{\max}$. However, the bath obviously modifies all the electronic energy gaps and induces nonadiabatic transitions so that the depopulation of the ground state is not complete anymore. Short pulses and thus large amplitudes are then expected to be more efficient to prepare a selected excited state and recover more population in the acceptor. For instance, a pulse duration of 13fs involves large maximal amplitudes, $A_y = 2.875 \times 10^{-3}$ a.u. and $A_z = 5.4739 \times 10^{-3}$ a.u. but for a short time. For a linear polarization along Oy, the $E_0 \rightarrow E_2$ transition is a two-state case. Without interaction with the bath, the π-pulse always populates the E_2 state with a yield of 100%. However, for a linear polarization along Oz, the detuned transition $E_0 \rightarrow E_1$ transition may interfere and modify the prediction of the two-state model, when the field amplitude increases. The perturbation remains very weak for a pulse duration longer than about 50 fs but is strong for short pulses of about 10 fs leading to a yield of only 50%.

An interesting alternative is a chirped pulse[107,108] for which the carrier frequency is linearly varying in time:

$$\mathcal{E}_{y/z}(t) = \mathcal{A}_{y/z}(t) \cos\left(\omega_{y/z}(t)t + \phi_{y/z}\right). \qquad (23)$$

with $\omega_{y/z}(t) = \omega_{0,y/z} \pm \alpha_{y/z}t$. The parameters $\omega_{0,y/z}$ and $\alpha_{y/z}$ are chosen so that $\omega_{y/z}(\tau_{max}/2)$ is the resonance frequency of each transition and the frequency variation during the pulse is 4% of the central frequency. These parameters have been chosen to remain rather realistic, in agreement with current chirped laser pulses[109]. Since the vibronic motion from the initial Franck-Condon geometry decreases the energy gap with the ground state, a decrease of the frequency is expected to favor the transition by following the vibrational wave packet[110,111]. We actually observed that a positive chirp is effectively less efficient. In every case, the amplitudes $A_{y/z}$ are those adopted for the corresponding π-pulses.

Figure 10 gives the final yield in the acceptor obtained with different τ_{max} for the π and positive or negative chirps with the two polarizations preparing E_2 or E_3 respectively. The yield would be 100% if the excited target state was reached and the ground state was completely depopulated. A decrease of the yield results solely from the bath in the case of the $E_0 \rightarrow E_2$ transition, with polarization Oy (thick blue line for the π-pulse and long dashes for the negative chirp and small dashes for the positive chirp). The yield decreases with τ_{max} in every case when E_2 is prepared. It presents a weak maximum for E_3. The positive chirp is less efficient than a negative chirp or a π-pulses.

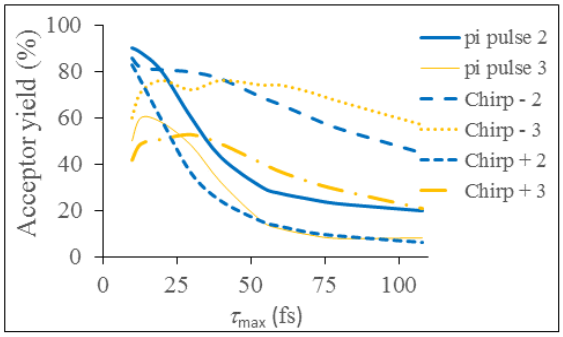

Figure 10. Comparison of the final yield in the acceptor state as a function of the pulse duration τ_{max} in the presence of the interaction with the baths. The system is prepared in the donor states E_2 or E_3 by a π-pulse (Eq. 21) (full lines, thick blue : E_2, thin orange : E_3), or by a negative chirp (Eq.(23)) (long blue dashes: E_2, orange dots: E_3), or by a positive chirp (small blue dashes : E_2, orange long dashes and dots: E_3).

B. Preparation of a superposed state

The preparation of a superposed state has already been discussed in the two-state case with a $\pi/2$-pulse or in the Λ type three-state model using a F-STIRAP (Fractional-STIRAP)[41]. However, these situations differ from our goal since in these applications the initial state is included in the final superposed state. Our objective in the V-type system is to depopulate the initial ground state and create a superposition of the excited states. The preparation of an excited superposition from a ground state by one or two few-cycle laser pulses with CEP (Carrier Envelope Phase) control has also been discussed with respect to the stationary or non-stationary character of the initial state[38].

In this work, we first generalize the π-pulse scheme to a $\pi/\sqrt{2}$-pulse condition to prepare a target superposition $|\pm\rangle = (|2\rangle \pm |3\rangle)/\sqrt{2}$ in the three-state V-type system. We show in Appendix B, that applying two equal duration pulses with the same Rabi frequency (*i.e.,* amplitudes in the inverse ratio of the dipole matrix elements) leads to this objective. The requirement to be fulfilled is that the integral of the Rabi frequency is equal to $\pi/\sqrt{2}$. Both polarizations along Oy and Oz are involved and the perturbations due to interference with the detuned transition, or due to the bath, still hinder the complete depletion of the ground state. The choice of the phase difference $\phi_z - \phi_y = 0$ or π provides the combination with plus or minus sign and therefore the excess of population is located in one or the other well. The creation of a superposition is illustrated in Fig. 11. Without the bath, the long pulse of about 50 fs (panel (a)) is in agreement with the predictions of the three-state V-model. The population of both excited states increases simultaneously and reaches 0.5 with complete depletion of the ground state. For the short pulse of 13fs (panel (b)), the interference with the acceptor state due to the polarization along Oz decreases the efficiency of the transition by leaving 20% in the ground state. However, the coherent superposition is still formed. As expected, the bath quickly destroys the superposition for

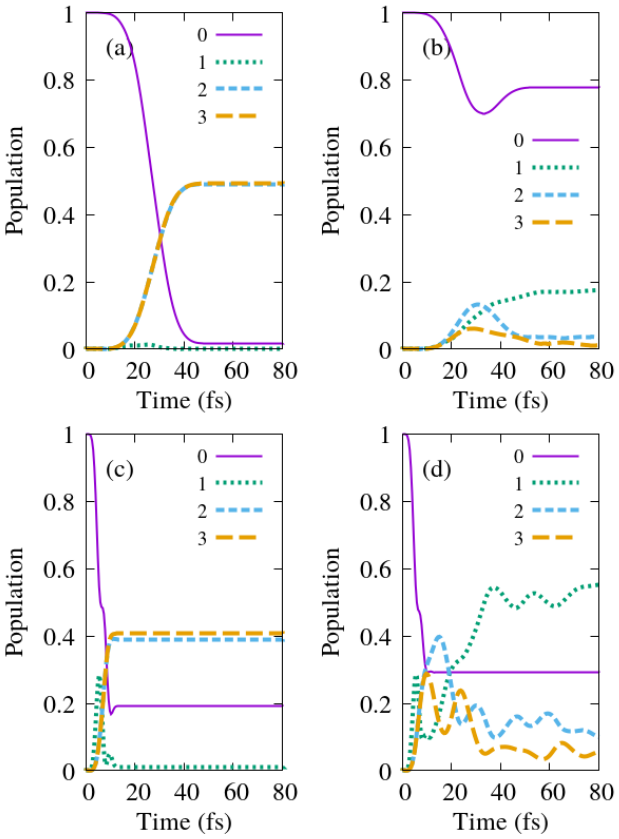

Figure 11. Adiabatic populations as a function of time when the system is excited in a superposition of donor states $|\pm\rangle = (|2\rangle \pm |3\rangle)/\sqrt{2}$ by $\pi/\sqrt{2}$ pulses. Panel (a): 54fs without bath, panel (b): 54fs with bath, panel (c): 13fs without bath, panel (d): 13fs with bath. The color code is the same as in Fig.7.

the long pulse.

We now compare with two slightly different strategies by focusing only on short excitation since it is already seen in section IV that coherence and dissymetry effect have a short lifetime in this molecular system. In the forthcoming examples, we keep the values of the maximal amplitudes $A_{y/z}$.

First, we compare with an elliptical polarization to create the superposed state. The field is:

$$\mathcal{E}(t) = \mathcal{A}_y(t)\cos(\omega t) \pm \mathcal{A}_z(t)\sin(\omega t) \qquad (24)$$

with a single frequency taken as the average of the two frequencies in resonance with the donor states $\omega = (\omega_{02} + \omega_{03})/2$. In the bath free situation, due to a slight detuning of both transitions, the $\pi/\sqrt{2}$-pulse strategy does not perfectly works. By optimizing the amplitude A_y, which is here multiplied by a factor 1.25, a superposition is created as shown in panel (a) of Fig. 12. The evolution is then similar to that obtained with the two linearly polarized pulses without the bath (see Figs.12(a) and 11(c), or with the bath (see Figs. 12(b) and 11(d).

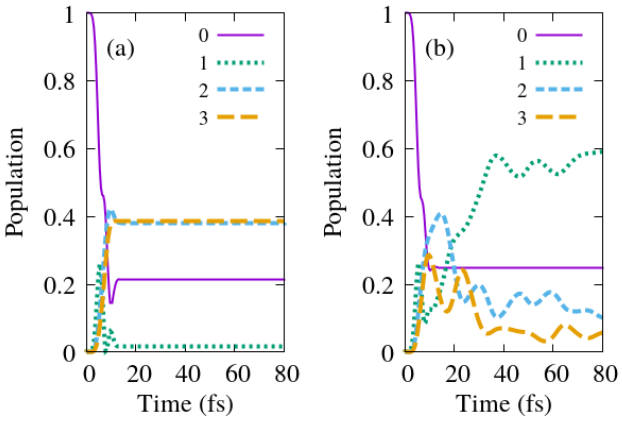

Figure 12. Adiabatic populations as a function of time when the system is excited in a superposition of donor states $|\pm\rangle = (|2\rangle \pm |3\rangle)/\sqrt{2}$ by an elliptically polarized pulse (Eq.(24)) of 13fs. Panel (a): without bath, panel (b): with bath. The amplitude A_y is multiplied by a factor 1.25 with respect to the $\pi/\sqrt{2}$-pulse condition, while A_z fulfills this condition. The color code is the same as in Fig.7.

Figure 13 displays two examples of superposition created with a chirped pulse. In the absence of the bath, the long pulse (54fs) is as efficient as the $\pi/\sqrt{2}$ strategy, but the short pulse induces a stronger interference with the acceptor state. The survival time of the superposition remains longer for the short pulse.

Finally, we compare the local dissymmetry, which could be temporarily observed by populating the D_R and D_L right or left donor sites. One or the other sides are reached by imposing phases 0 or π respectively for the field polarized along the Oz axis. Fig.14 gathers the different situations examined in this work and presents the sum of the average values of the collective coupling mode in each localized diabatic state. One observes that the effect is more important when one simply assumes an initial Franck-Condon preparation, in other words an impulsive pulse. Both $\pi/\sqrt{2}$ and chirped pulses create a transitory dissymmetry but there is a delay due to the finite duration of the pulses and the baths already interfere during the interaction with the light, thus blurring the effect. As already mentioned, in this molecular system, the characteristic timescale over which the dissymetry holds does not exceed about 10 fs. The lifetime of the created electronic coherence is thus very short to induce a measurable effect on the overall population dynamics.

VI. CONCLUSION

This work brings two original contributions to the abundantly explored domain of dendrimer photophysics. The first one illustrates how to build a realistic model dealing with open quantum system dynamics from *ab initio* data at a high level of theory for a

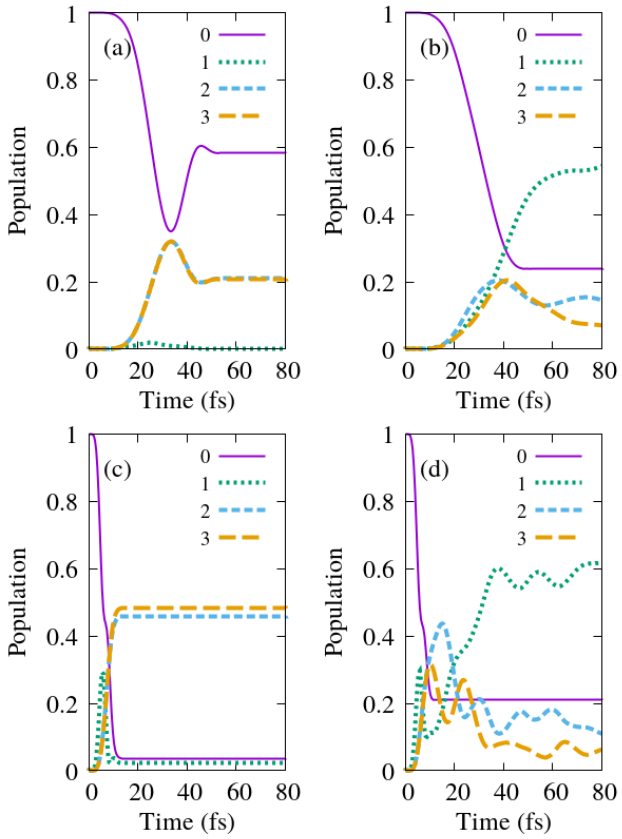

Figure 13. Adiabatic populations as a function of time when the system is excited in a superposition of donor states $|\pm\rangle = (|2\rangle \pm |3\rangle)/\sqrt{2}$ by pulses with a negative chirp (Eq.(23)). Panel (a): 54fs without bath, panel (b): 54fs with bath, panel (c): 13fs without bath, panel (d): 13fs with bath. The amplitudes A_y and A_z are those of the $\pi/\sqrt{2}$-pulse condition. The color code is the same as in Fig.7.

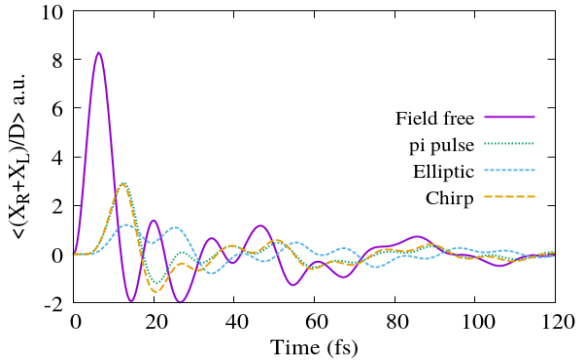

Figure 14. Time-evolution of the sum of the average values of the collective vibrational modes (Eqs.(18) and (19)) in the localized diabatic states D_R and D_L when the system is prepared in a superposition $|+\rangle = (|2\rangle + |3\rangle)/\sqrt{2}$ of the two donor eigenstates E_2 and E_3. Solid magenta line: initialization without field (see Fig.7(c)), green dots : two $\pi/\sqrt{2}$-pulses of 13 fs duration (see Fig.11(d)), cyan dashes : pulse with elliptic polarization ensuring the best creation of the superposition in the bath free case (see Fig.12 (b)), orange long dashes : pulse with negative chirp (Eq.(23)) (see Fig.13(d)).

complex system with conical intersections involving several tuning and coupling vibrational baths. The second one concerns the analysis of the coherent preparation by short laser pulses of excited donor states and most particularly of their superposition[27]. Initial conditions in excited states are usually assumed without explicit simulations of this preparation with fields.

The model is inspired from a trimer of phenylene ethynylene for which a complete *ab initio* investigation is currently in progress. The molecular system is particularly interesting because the early relaxation dynamics obviously involves some skeletal vibrational modes in a small isolated frequency region related to the triple bond in-plane vibrations. We are confident that the model is realistic and well adapted to describe the main early dynamical processes. The second peculiarity of the trimer is the structure of its transition dipole matrix towards the donor states. More precisely, the dipole moments towards two particular donor states being orthogonal, offer the possibility to address them by different polarized waves.

Kassal *et al.*[39,112] have drawn attention on this interesting property in recent reports about a two-site excitonic system with orthogonal transition dipoles in which an enhancement of excitation transfer should be possible by exciting a left or right donor site, *i.e.*, by preparing a particular superposition of the delocalized eigenstates. This situation with orthogonal dipoles differs from the case with alignment of the transition dipole moments, which is a condition for long-lived quasi stationary coherence in a V-type system driven by incoherent light[32]. In order to individually address a localized D_R or D_L site, we have proposed two strategies based on $\pi/\sqrt{2}$-pulses with linear or elliptic polarization to prepare the superposition in an electronic V-type system. This presents the potentiality to be transposed to other molecular systems. In the present example, we have analyzed the effect of a perturbation by a detuned transition within the frame of an environment provided by the vibrational tuning and coupling baths. In the present case, the initial local dissymmetry linked to the created coherence of the superposition survives for only about 10-15 fs. The occupation of the selected site is very short and does not improve the transfer towards the acceptor when this is compared to the case where a single delocalized eigenstate is populated or to a mixed state. Due to the high symmetry of the model and of the Franck-Condon geometry, the population evolutions are the same for an equally weighted superposition or for the corresponding mixed state. This may be verified by wave packet propagation. A difference appears only when the two localized sites are not symmetrical, as assumed in Kassal's proposition[39]. In a symmetric system, the creation of the dissymmetry cannot be detected in the population but probably in time-resolved anisotropy decay[48]. The coherence and the dissymmetry in the behavior of the collective coupling mode could be modified by varying some parameters. In particular, the increase or decrease of the coupling between the two

donor states brings closer or separate the two wells of the adiabatic lower donor state. Doubling the donor-donor coupling allows several oscillations during about 50fs in the localized site populated by the superposed state. On the contrary, modifying the coupling with the acceptor, as it is illustrated in the supporting information, does not modify the timescale of the created dissymmetry. Finally, the most important system parameter to modify is the symmetry of the system. Functionalizing one of the trimer branches might allow to better enhance the local dissymetry process corresponding to diabatic localization and finally funnel the exciton transfer. To reach that goal, the energy gap between acceptor and donor states should be greater. Such functionalized systems can be investigated with the very same quantum chemistry computations proposed in this work.

Both π and chirped pulses have also been discussed for populating excited states. If we disregard the direct radiative excitation of E_1, the acceptor is only populated thanks to the baths (except for very short excitation, for instance with a π-pulse in Fig.11 or with a chirped one in Fig.13). Some chirp strategies prove to be more favorable, to populate E_1, in the presence of the baths.

Even though the model based on *ab initio* data of the chosen molecular system is not perfectly adapted to illustrate the dissymetry effect, we have proposed two strategies when the donor eigenstates couple to laser modes with different polarization to prepare the superposition in an electronic V-type system. This presents the potentiality to be transposed to other molecular systems. Functionalizing one of the trimer branches might allow to better enhance the local dissymmetry process corresponding to diabatic localization and finally funnel the exciton transfer. To reach that goal, the energy gap between acceptor and donor states should be greater. Such functionalized systems can be investigated with the very same quantum chemistry computations proposed in this work.

With laser pulses of about 15fs, one observes a delay in the occupation of the localized sites of about 5fs and therefore a reduction of the motion amplitude due to the effect of the baths. If the target is to increase the lifetime of the asymmetry and thus of the coherence, other strategies should be tried, for instance, ultra-short attosecond pulses[113,114], short half-cycle pulses[38], succession of kick pulses already used for molecular orientation and alignment[115], light-induced nonadiabaticity[116], Floquet engineering[117,118] or exploit the optimal control tools with environment[119] or deap learning new proposals[120].

SUPPLEMENTARY MATERIAL

The supplemental material gives the Cartesian coordinates of the atoms at the ground state equilibrium geometry computed at the CAM-B3LYP/6-31+G* level of theory. It presents some complementary examples of electronic dynamics, in particular the effect of the variation of the coupling between A and D_2. We also verify the stability of the early dynamics with respect to the spectral density range for the tuning baths.

ACKNOWLEDGMENTS

This work has been performed within the French GDR 3575 THEMS. GB is grateful to the French MENRT ((French Ministry of Education Research and Technology) for funding his PhD grant.

DATA AVAILABILITY

The data that support this study are available on request from the authors.

Appendix A: Model parameters

The *ab initio* matrices of the permanent dipole and transition dipoles along the axes Oy and Oz (see Fig.1) and in the adiabatic representation are (in a.u.):

$$\mu_{\mathbf{y}} = \begin{pmatrix} 0 & 0 & 3.8576 & 0 \\ 0 & 0 & 0 & 0 \\ 3.8576 & 0 & 0 & 0 \\ 0 & 0 & 0 & 0 \end{pmatrix} \tag{A1}$$

and

$$\mu_{\mathbf{z}} = \begin{pmatrix} 0.0201 & 5.0307 & 0 & 1.5324 \\ 5.0307 & 0.4325 & 0 & 0 \\ 0 & 0 & -0.0990 & 0 \\ 1.5324 & 0 & 0 & -0.2799 \end{pmatrix} \tag{A2}$$

The spectral densities parameters are gathered in Table I.

Table I. Parameters for spectral density $\mathcal{J}(\omega)$ (Eq.(12)).

J_k or $J_{kk'}$	p_j (a.u)	Ω_j (a.u)	Γ_j (a.u)
J_A	3.51×10^{-10}	1.07542×10^{-2}	2.7879×10^{4}
J_{D_2}	2.93×10^{-10}	1.07952×10^{-2}	2.7879×10^{4}
$J_{D_2D_3}$	2.11×10^{-10}	1.07907×10^{-2}	2.7879×10^{4}
J_{AD_2}	6.32×10^{-11}	1.07907×10^{-2}	2.7879×10^{4}

We consider that the baths making fluctuate states D_2 and D_3 are correlated with $J_{D_3} = 0.6 J_{D_2}$.

Appendix B: Preparation by two $\pi/\sqrt{2}$-pulses

The two carrier frequencies ω_{0k} with k=2,3 are in resonance with the energy gaps. They have sine square envelopes as specified in Eq.(22) and the same duration τ_{max}:

$$\mathcal{E}(t) = \mathcal{A}_{0x}(t)\cos(\omega_{02}t) + \mathcal{A}_{0y}(t)\cos(\omega_{03}t). \tag{B1}$$

The amplitudes are chosen to get the same Rabi frequency $\Omega_{y/z}(t) = \mu_{y/z}\mathcal{A}_{y/z}(t)$, *i.e.*, $A_{0y}/A_{0z} = \mu_{03}/\mu_{02}$. In the resonant case, the coupled equations in a three-state system expressed in the interaction representation and within the rotating wave approximation depend on an effective Hamiltonian:

$$H_{eff}(t) = -\hbar/2 \begin{pmatrix} 0 & \Omega_{02}(t) & \Omega_{03}(t) \\ \Omega_{02}(t) & 0 & 0 \\ \Omega_{03}(t) & 0 & 0 \end{pmatrix}. \quad \text{(B2)}$$

The eigenvalues are $\Omega_0 = 0$ and $\Omega_\pm(t) = \pm\hbar\sqrt{\Omega_{02}^2(t) + \Omega_{03}^2(t)}/2$. The eigenvectors are parameterized by an angle $\tan\theta(t) = \Omega_{02}(t)/\Omega_{03}(t)$:

$$\begin{aligned} |\Psi_0\rangle &= -\cos\theta\,|2\rangle + \sin\theta\,|3\rangle \\ |\Psi_+\rangle &= \frac{1}{\sqrt{2}}\left(-|0\rangle + \sin\theta\,|2\rangle + \cos\theta\,|3\rangle\right) \\ |\Psi_-\rangle &= \frac{1}{\sqrt{2}}\left(|0\rangle + \sin\theta\,|2\rangle + \cos\theta\,|3\rangle\right). \end{aligned} \quad \text{(B3)}$$

When the Rabi frequencies are equal, $\Omega_{02}(t) = \Omega_{03}(t) = \Omega(t)$, one have $\Omega_\pm(t) = \pm\hbar\sqrt{2}\Omega(t)/2$ and $\sin\theta(t) = \cos\theta(t) = 1/\sqrt{2}$. By expressing the evolution operator in terms of the adiabatic eigenvalues and eigenstates[121,122]:

$$\begin{aligned} U(t,0) &= |\Psi_0\rangle\langle\Psi_0| \\ &+ |\Psi_-\rangle\, e^{-\frac{i}{\hbar}\int_0^t \Omega_-(t')dt'}\langle\Psi_-| \\ &+ |\Psi_+\rangle\, e^{-\frac{i}{\hbar}\int_0^t \Omega_+(t')dt'}\langle\Psi_+| \end{aligned} \quad \text{(B4)}$$

the probabilities $P_{j0}(t) = |\langle j|\,U(t,0)\,|0\rangle|^2$ are given by:

$$P_{00}(t) = \cos^2\left(\sqrt{2}/2\int_0^t \Omega(t')dt'\right) \quad \text{(B5)}$$

and

$$P_{20}(t) = P_{30}(t) = \frac{1}{2}\sin^2\left(\sqrt{2}/2\int_0^t \Omega(t')dt'\right). \quad \text{(B6)}$$

One gets $P_{20}(\tau_{\max}) = P_{30}(\tau_{\max}) = 1/2$ when $\int_0^{\tau_{\max}}\Omega(t')dt' = \pi/\sqrt{2}$.

This solution may be derived also from the coupled equations with the Hamiltonian (Eq.(B2)) by imposing that the two Rabi frequencies are equal :

$$\begin{pmatrix} \dot{b}_0(t) \\ \dot{b}_2(t) \\ \dot{b}_3(t) \end{pmatrix} = \frac{i}{2}\begin{pmatrix} 0 & \Omega(t) & \Omega(t) \\ \Omega(t) & 0 & 0 \\ \Omega(t) & 0 & 0 \end{pmatrix}\begin{pmatrix} b_0(t) \\ b_2(t) \\ b_3(t) \end{pmatrix}. \quad \text{(B7)}$$

This leads to the equation

$$\ddot{b}_0 - \frac{\dot{\Omega}}{\Omega}\dot{b}_0 + \frac{1}{2}\Omega^2 b_0 = 0. \quad \text{(B8)}$$

By changing the variable $z(t) = \frac{1}{2}\int_{-\infty}^t \Omega(t')dt'$ as suggested in Ref.[105] for the $\pi-$pulse, one gets, by denoting $b_0^{'} = \partial b_0/\partial z$:

$$\dot{z}^2 b_0^{''} + \ddot{z} b_0^{'} - \frac{\dot{\Omega}}{\Omega}\dot{z} b_0^{'} + \frac{1}{2}\Omega^2 b_0 = 0. \quad \text{(B9)}$$

After simplification, taking into account $\dot{z} = \Omega/2$ and $\ddot{z} = \dot{\Omega}/2$, one has:

$$b_0^{''} + 2b_0 = 0. \quad \text{(B10)}$$

The general solution is $b_0(z) = C\cos\left(\sqrt{2}z\right) + D\sin\left(\sqrt{2}z\right)$. By imposing the initial conditions $b_0(0) = C = 1$ and $b_0^{'}(0) = \sqrt{2}D = 0$, one recovers the expressions of $P_{00}(t)$ and $P_{02}(t)$ (Eqs.(B5) and (B6)).

[1] L. Valkunas *et al.*, *Photosynthetic excitons* (World Scientific, 2000).
[2] R. E. Blankenship, *Molecular mechanisms of photosynthesis* (John Wiley & Sons, 2014).
[3] G. D. Scholes, G. R. Fleming, A. Olaya-Castro, and R. Van Grondelle, Nat. Chemistry **3**, 763 (2011).
[4] G. D. Scholes, G. R. Fleming, L. X. Chen, A. Aspuru-Guzik, A. Buchleitner, D. F. Coker, G. S. Engel, R. van Grondelle, A. Ishizaki, D. M. Jonas, J. S. Lundeen, J. K. McCusker, S. Mukamel, J. P. Ogilvie, A. Olaya-Castro, M. A. Ratner, F. C. Spano, K. B. Whaley, and X. Zhu, Nature **543**, 647 (2017).
[5] T. Mančal, Chem. Phys. **532**, 110663 (2020).
[6] J.-L. Brédas, E. H. Sargent, and G. D. Scholes, Nat. materials **16**, 35 (2017).
[7] C. Creatore, M. A. Parker, S. Emmott, and A. W. Chin, Phys. Rev. Lett. **111**, 253601 (2013).
[8] L. Chen, P. Shenai, F. Zheng, A. Somoza, and Y. Zhao, Molecules **20**, 15224 (2015).
[9] M. Cainelli and Y. Tanimura, J. Chem. Phys. **154**, 034107 (2021).
[10] H.-G. Duan, V. I. Prokhorenko, R. J. Cogdell, K. Ashraf, A. L. Stevens, M. Thorwart, and R. D. Miller, Proceedings of the National Academy of Sciences **114**, 8493 (2017).
[11] V. I. Novoderezhkin, E. Romero, J. Prior, and R. van Grondelle, Phys. Chem. Chem. Phys. **19**, 5195 (2017).
[12] A. Kolli, E. J. O'Reilly, G. D. Scholes, and A. Olaya-Castro, J. Chem. Phys. **137**, 174109 (2012).
[13] A. Chin, J. Prior, R. Rosenbach, F. Caycedo-Soler, S. Huelga, and M. Plenio, Nat. Physics **9**, 113 (2013).
[14] F. Ma, E. Romero, M. R. Jones, V. I. Novoderezhkin, and R. van Grondelle, Nat. Commun. **10**, 933 (2019).
[15] A. Niedringhaus, V. R. Policht, R. Sechrist, A. Konar, P. D. Laible, D. F. Bocian, D. Holten, C. Kirmaier, and J. P. Ogilvie, Proceedings of the National Academy of Sciences **115**, 3563 (2018).
[16] A. Ishizaki, T. R. Calhoun, G. S. Schlau-Cohen, and G. R. Fleming, Phys. Chem. Chem. Phys. **12**, 7319 (2010).
[17] C. Kreisbeck and T. Kramer, J. Phys. Chem. Lett. **3**, 2828 (2012), arXiv:1203.1485.

[18] J. Strümpfer and K. Schulten, J. Chem. Phys. **137**, 065101 (2012).
[19] S.-H. Yeh, J. Zhu, and S. Kais, J. Chem. Phys. **137**, 084110 (2012).
[20] M. F. Gelin and W. Domcke, J. Chem. Phys. **144**, 194104 (2016).
[21] H.-P. Breuer and F. Petruccione, *The Theory of Open Quantum Systems* (Oxford University Press, 2002).
[22] U. Weiss, *Quantum Dissipative Systems* (Singapore, World Scientific, 2012).
[23] I. de Vega and D. Alonso, Rev. Mod. Phys. **89**, 015001 (2017).
[24] L. Chen, M. F. Gelin, V. Y. Chernyak, W. Domcke, and Y. Zhao, Faraday Discuss. **194**, 61 (2016).
[25] H.-G. Duan and M. Thorwart, J. Phys. Chem. Lett. **7**, 382 (2016).
[26] A. G. Dijkstra and V. I. Prokhorenko, J. Chem. Phys. **147**, 064102 (2017).
[27] C. Arnold, O. Vendrell, R. Welsch, and R. Santra, Phys. Rev. Lett. **120**, 123001 (2018).
[28] B. G. Levine, M. P. Esch, B. S. Fales, D. T. Hardwick, W.-T. Peng, and Y. Shu, Annu. Rev. Phys. Chem. **70**, 21 (2019).
[29] E. C. Wu, Q. Ge, E. A. Arsenault, N. H. C. Lewis, N. L. Gruenke, M. J. Head-Gordon, and G. R. Fleming, Phys. Chem. Chem. Phys. **21**, 14153 (2019).
[30] E. Mangaud, B. Lasorne, O. Atabek, and M. Desouter-Lecomte, J. Chem. Phys. **151**, 244102 (2019).
[31] T. Mančal and L. Valkunas, New J. Phys. **12**, 065044 (2010).
[32] T. V. Tscherbul and P. Brumer, Phys. Rev. Lett. **113**, 113601 (2014).
[33] A. Chenu and P. Brumer, J. Chem. Phys. **144**, 044103 (2016).
[34] A. Dodin, T. V. Tscherbul, and P. Brumer, J. Chem. Phys. **145**, 244313 (2016).
[35] T. V. Tscherbul and P. Brumer, J. Chem. Phys. **148**, 124114 (2018).
[36] V. Janković and T. Mančal, J. Chem. Phys. **153**, 244110 (2020).
[37] J. D. Roscioli, S. Ghosh, A. M. LaFountain, H. A. Frank, and W. F. Beck, J. Phys. Chem. Lett. **9**, 5071 (2018).
[38] W. Hu, B. Gu, and I. Franco, J. Chem. Phys. **152**, 184305 (2020).
[39] S. Tomasi, S. Baghbanzadeh, S. Rahimi-Keshari, and I. Kassal, Phys. Rev. A **100**, 043411 (2019).
[40] A. G. Dijkstra and A. Beige, J. Chem. Phys. **151**, 034114 (2019).
[41] N. V. Vitanov, A. A. Rangelov, B. W. Shore, and K. Bergmann, Rev. Mod. Phys. **89**, 015006 (2017).
[42] E. Y. Poliakov, V. Chernyak, S. Tretiak, and S. Mukamel, J. Chem. Phys. **110**, 8161 (1999).
[43] J. C. Kirkwood, C. Scheurer, V. Chernyak, and S. Mukamel, J. Chem. Phys. **114**, 2419 (2001).
[44] R. Kishi, T. Minami, H. Fukui, H. Takahashi, and M. Nakano, J. Chem. Phys. **128**, 244306 (2008).
[45] S. Fernandez-Alberti, V. D. Kleiman, S. Tretiak, and A. E. Roitberg, J. Phys. Chem. A **113**, 7535 (2009).
[46] J. L. Palma, E. Atas, L. Hardison, T. B. Marder, J. C. Collings, A. Beeby, J. S. Melinger, J. L. Krause, V. D. Kleiman, and A. E. Roitberg, J. Phys. Chem. C **114**, 20702 (2010).
[47] J. Huang, L. Du, D. Hu, and Z. Lan, Journal of Computational Chemistry **36**, 151 (2015).
[48] D. Ondarse-Alvarez, S. Kömürlü, A. E. Roitberg, G. Pierdominici-Sottile, S. Tretiak, S. Fernandez-Alberti, and V. D. Kleiman, Phys. Chem. Chem. Phys. **18**, 25080 (2016).
[49] T. Nelson, S. Fernandez-Alberti, A. E. Roitberg, and S. Tretiak, J. Phys. Chem. Lett. **8**, 3020 (2017).
[50] M. C. Aguilera, A. E. Roitberg, V. D. Kleiman, S. Fernandez-Alberti, and J. F. Galindo, J. Phys. Chem. C **124**, 22383 (2020).
[51] E. K.-L. Ho and B. Lasorne, Computational and Theoretical Chemistry **1156**, 25 (2019).
[52] A. Garg, J. N. Onuchic, and V. Ambegaokar, J. Chem. Phys. **83**, 4491 (1985).
[53] M. Thoss, H. Wang, and W. H. Miller, J. Chem. Phys. **115**, 2991 (2001).
[54] J. Cao and G. A. Voth, J. Chem. Phys. **106**, 1769 (1997).
[55] K. H. Hughes, C. D. Christ, and I. Burghardt, J. Chem. Phys. **131**, 124108 (2009).
[56] M. Tanaka and Y. Tanimura, J. Chem. Phys. **132**, 214502 (2010).
[57] A. Chenel, E. Mangaud, I. Burghardt, C. Meier, and M. Desouter-Lecomte, J. Chem. Phys. **140**, 044104 (2014).
[58] M. P. Woods, R. Groux, A. W. Chin, S. F. Huelga, and M. B. Plenio, J. Math. Phys. **55**, 032101 (2014).
[59] J. Iles-Smith, N. Lambert, and A. Nazir, Phys. Rev. A **90**, 032114 (2014).
[60] J. Iles-Smith, A. G. Dijkstra, N. Lambert, and A. Nazir, J. Chem. Phys. **144**, 044110 (2016).
[61] H. Wang and M. Thoss, J.Chem. Phys. **119**, 1289 (2003).
[62] F. Di Maiolo, D. Brey, R. Binder, and I. Burghardt, J. Chem. Phys. **153**, 184107 (2020).
[63] A. M. Alvertis, F. A. Y. N. Schröder, and A. W. Chin, J. Chem. Phys. **151**, 084104 (2019).
[64] J. Sun, B. Luo, and Y. Zhao, Phys. Rev. B **82**, 014305 (2010).
[65] Y. Ke and Y. Zhao, J. Chem. Phys. **146**, 174105 (2017).
[66] K. Nakamura and Y. Tanimura, Phys. Rev. A **98**, 012109 (2018).
[67] Y. Tanimura and R. Kubo, J. Phys. Soc. Jpn. **58**, 101 (1989).
[68] A. Ishizaki and Y. Tanimura, J. Phys. Soc. Jpn. **74**, 3131 (2005).
[69] A. Ishizaki and G. R. Fleming, J. Chem. Phys. **130**, 234111 (2009).
[70] Q. Shi, L. Chen, G. Nan, R.-X. Xu, and Y. Yan, J. Chem. Phys. **130**, 084105 (2009).
[71] H. Liu, L. Zhu, S. Bai, and Q. Shi, J. Chem. Phys. **140**, 134106 (2014).
[72] Y. Tanimura, J. Chem. Phys. **153**, 020901 (2020).
[73] M. J. Frisch, G. W. Trucks, H. B. Schlegel, G. E. Scuseria, M. A. Robb, J. R. Cheeseman, G. Scalmani, V. Barone, G. A. Petersson, H. Nakatsuji, X. Li, M. Caricato, A. V. Marenich, J. Bloino, B. G. Janesko, R. Gomperts, B. Mennucci, H. P. Hratchian, J. V. Ortiz, A. F. Izmaylov, J. L. Sonnenberg, D. Williams-Young, F. Ding, F. Lipparini, F. Egidi, J. Goings, B. Peng, A. Petrone, T. Henderson, D. Ranasinghe, V. G. Zakrzewski, J. Gao, N. Rega, G. Zheng, W. Liang, M. Hada, M. Ehara, K. Toyota, R. Fukuda, J. Hasegawa, M. Ishida, T. Nakajima, Y. Honda, O. Kitao, H. Nakai, T. Vreven, K. Throssell, J. A. Montgomery, Jr., J. E. Peralta, F. Ogliaro, M. J. Bearpark, J. J. Heyd, E. N. Brothers, K. N. Kudin, V. N. Staroverov, T. A. Keith,

R. Kobayashi, J. Normand, K. Raghavachari, A. P. Rendell, J. C. Burant, S. S. Iyengar, J. Tomasi, M. Cossi, J. M. Millam, M. Klene, C. Adamo, R. Cammi, J. W. Ochterski, R. L. Martin, K. Morokuma, O. Farkas, J. B. Foresman, and D. J. Fox, "Gaussian~16 Revision A.03," (2016), gaussian Inc. Wallingford CT.
[74] D. Jacquemin, B. Mennucci, and C. Adamo, Phys. Chem. Chem. Phys. **13**, 16987 (2011).
[75] E. K.-L. Ho, T. Etienne, and B. Lasorne, J. Chem. Phys. **146**, 164303 (2017).
[76] B. Gonon, A. Perveaux, F. Gatti, D. Lauvergnat, and B. Lasorne, J. Chem. Phys. **147**, 114114 (2017).
[77] R. L. Martin, J. Chem. Phys. **118**, 4775 (2003).
[78] M. Desouter-Lecomte, D. Dehareng, B. Leyh-Nihant, M. T. Praet, A. J. Lorquet, and J. C. Lorquet, J. Phys. Chem. **89**, 214 (1985).
[79] J. R. Reimers and N. S. Hush, Chem. Phys. **299**, 79 (2004).
[80] L. K. McKemmish, R. H. McKenzie, N. S. Hush, and J. R. Reimers, J. Chem. Phys. **135**, 244110 (2011).
[81] A. Kühl and W. Domcke, J. Chem. Phys. **116**, 263 (2002).
[82] L. S. Cederbaum, E. Gindensperger, and I. Burghardt, Phys. Rev. Lett. **94**, 113003 (2005).
[83] E. Gindensperger, I. Burghardt, and L. S. Cederbaum, J. Chem. Phys. **124**, 144103 (2006).
[84] R. Martinazzo, K. H. Hughes, F. Martelli, and I. Burghardt, Chem. Phys. **377**, 21 (2010).
[85] V. Chernyak and S. Mukamel, J. Chem. Phys. **105**, 4565 (1996), https://doi.org/10.1063/1.472302.
[86] I. Burghardt, R. Martinazzo, and K. H. Hughes, The Journal of Chemical Physics **137**, 144107 (2012).
[87] K. H. Hughes, B. Cahier, R. Martinazzo, H. Tamura, and I. Burghardt, Chemical Physics **442**, 111 (2014), papers from the 11th International Conference on Femtochemistry (FEMTO11) that took place at The Technical University of Denmark (DTU), Copenhagen.
[88] J. Strümpfer and K. Schulten, J. Chem. Phys. **134**, 095102 (2011).
[89] M. F. Gelin, L. Z. Sharp, D. Egorova, and W. Domcke, J. Chem. Phys. **136**, 034507 (2012).
[90] W. Popp, M. Polkehn, K. H. Hughes, R. Martinazzo, and I. Burghardt, J. Chem. Phys. **150**, 244114 (2019).
[91] R. Borrelli and M. F. Gelin, Sci. Rep. **7**, 9127 (2017).
[92] Q. Shi, Y. Xu, Y. Yan, and M. Xu, J. Chem. Phys. **148**, 174102 (2018).
[93] Y. Yan, M. Xu, T. Li, and Q. Shi, J. Chem. Phys. **154**, 194104 (2021).
[94] R. Martinazzo, K. H. Hughes, F. Martelli, and I. Burghardt, Chemical Physics **377**, 21 (2010).
[95] H. Tamura, R. Martinazzo, M. Ruckenbauer, and I. Burghardt, J. Chem. Phys. **137**, 22A540 (2012).
[96] C. Meier and D. J. Tannor, J. Chem. Phys. **111**, 3365 (1999).
[97] A. Pomyalov, C. Meier, and D. J. Tannor, Chem. Phys. **370**, 98 (2010).
[98] J. Hu, M. Luo, F. Jiang, R.-X. Xu, and Y. Yan, J. Chem. Phys. **134**, 244106 (2011).
[99] L. Cui, H.-D. Zhang, X. Zheng, R.-X. Xu, and Y. Yan, J. Chem. Phys. **151**, 024110 (2019).
[100] H. Rahman and U. Kleinekathöfer, J. Chem. Phys. **150**, 244104 (2019).
[101] L. Zhu, H. Liu, W. Xie, and Q. Shi, J. Chem. Phys. **137**, 194106 (2012).
[102] A. Chin, E. Mangaud, V. Chevet, O. Atabek, and M. Desouter-Lecomte, Chem. Phys. **525**, 110392 (2019).
[103] W. H. Press, S. A. Teukolsky, W. T. Vetterling, and B. P. Flannery, *Numerical Recipes - The Art of Scientific Computing* (Cambridge University Press, 1992).
[104] T. Nelson, S. Fernandez-Alberti, A. E. Roitberg, and S. Tretiak, Acc. Chem. Res. **47**, 1155 (2014).
[105] G. F. Thomas, Phys. Rev. A **27**, 2744 (1983).
[106] M. Holthaus and B. Just, Phys. Rev. A **49**, 1950 (1994).
[107] V. Malinovsky and J. Krause, Eur. Phys. J. D **14**, 147 (2001).
[108] S. Guérin, V. Hakobyan, and H. R. Jauslin, Phys. Rev. A **84**, 013423 (2011).
[109] A. M. Weiner, Review of Scientific Instruments **71**, 1929 (2000).
[110] J. Cao, C. J. Bardeen, and K. R. Wilson, J. Chem. Phys. **113**, 1898 (2000).
[111] V. V. Yakovlev, C. J. Bardeen, J. Che, J. Cao, and K. R. Wilson, J. Chem. Phys. **108**, 2309 (1998).
[112] S. Tomasi and I. Kassal, J. Phys. Chem. Lett. **11**, 2348 (2020).
[113] D. Haase, G. Hermann, J. Manz, V. Pohl, and J. C. Tremblay, Symmetry **13**, 205 (2021).
[114] M. A. Robb, A. J. Jenkins, and M. Vacher, in *Attosecond Molecular Dynamics* (The Royal Society of Chemistry, 2018) pp. 275–307.
[115] D. Sugny, A. Keller, O. Atabek, D. Daems, C. M. Dion, S. Guérin, and H. R. Jauslin, Phys. Rev. A **69**, 033402 (2004).
[116] C. Fábri, G. J. Halász, L. S. Cederbaum, and A. Vibók, J. Chem. Phys. **154**, 124308 (2021).
[117] N. Thanh Phuc and A. Ishizaki, J. Phys. Chem. Lett. **9**, 1243 (2018).
[118] N. T. Phuc and A. Ishizaki, Phys. Rev. B **99**, 064301 (2019).
[119] E. Mangaud, R. Puthumpally-Joseph, D. Sugny, C. Meier, O. Atabek, and M. Desouter-Lecomte, New J. Phys. **20**, 043050 (2018).
[120] I. Paparelle, L. Moro, and E. Prati, Phys. Lett. A **384**, 126266 (2020).
[121] A. Leclerc, D. Viennot, G. Jolicard, R. Lefebvre, and O. Atabek, Phys. Rev. A **94**, 043409 (2016).
[122] A. Leclerc, D. Viennot, G. Jolicard, R. Lefebvre, and O. Atabek, J. Phys. B: At. Mol. Opt. Phys. **50**, 234002 (2017).